Eur. Phys. J. B **55**, 29–36 (2007)
DOI: 10.1140/epjb/e2007-00037-3

THE EUROPEAN PHYSICAL JOURNAL B

BEEM spectra of various Au-Si samples and their analysis

A. Thiaville[a], F. Caud, C. Vouille, and J. Miltat

Laboratoire de Physique des Solides, CNRS, Univ. Paris-Sud, 91405 Orsay Cedex, France

Received 15 September 2006
Published online 7 February 2007 –

Abstract. Ballistic electron emision microscopy spectra have been measured at room temperature on Au films deposited on the Si(111)-H surface by different procedures. In order to analyze them in detail, we propose a fully analytical description of these spectra, directly based on the phase-space model of Bell and Kaiser. This allows fitting experimental data over a wide voltage range, comprising the threshold and the quasi-linear regions. Two main independent parameters are extracted from the fits, namely the effective Schottky barrier height and hot-electron transmission of the sample. These show a clear variation with sample preparation conditions.

PACS. 68.37.Uv Near-field scanning microscopy and spectroscopy – 73.40.Qv Metal-insulator-semiconductor structures (including semiconductor-to-insulator) – 72.15.-v Electronic conduction in metals and alloys

1 Introduction

In Ballistic electron emission microscopy (BEEM) [1], the transmission of hot electrons injected by a tunneling tip across a metallic base film at non-zero bias and into a semiconductor substrate (through the Schottky barrier), is measured as a function of position and tunnel voltage. The method was initially described as providing [1] *a direct probe of interface electronic structure, including the important Schottky barrier height, quantum-mechanical reflection of electrons at the interface, and ballistic electron transport properties of the base film.* These topics were intensively developed in the following years [2,3], through additional experiments and increasing refinements of the BEEM current models.

The initial model [4] considered only the conservation, at the metal-semiconductor interface, of the electrons' energy and momentum parallel to the interface. The electrons were described in the free electrons approximation with an effective mass, and quantum mechanical transmission coefficients of the current were discarded. Close to the voltage threshold (the Schottky barrier height) and at zero temperature, this model evaluates the BEEM current normalized to the injected tunnel current as a square law of the voltage excess. This model was later refined [5] by the introduction of the wave transmission coefficients of the electrons at the metal-semiconductor interface. This results into a power law with an exponent 5/2 close to the threshold. Therefore BEEM spectra are often fitted, around the threshold region, by a simple power law

$$I_{\mathrm{B}}/I_{\mathrm{T}} = A\,(V - V_0)^n\,. \tag{1}$$

As the measured BEEM current varies quasi-linearly with voltage ≈0.2 V above threshold, it is clear that this approach is not fully satisfactory. For example, it was reported that the extracted threshold V_0 depends on the power index n [6]. Alternatively, effective Schottky barriers were also evaluated by linear regression [7]. In contrast to these simplistic approaches, more complex numerical models have been proposed, and even Monte-Carlo calculations of the electrons scattering have been developed. These models contain several additional parameters, such as scattering probabilities, and allow incorporating the full complexity of the real band structure of the metal and semiconductor. The number of the parameters is however an obstacle to fitting the experimental data and extracting reliably meaningful physical parameters.

With the recent development of Ballistic emission magnetic microscopy (BEMM) [8], where the ballistic electron transport across a spin-valve metallic base is the magnetic contrast source, the need for an easy yet precise evaluation of BEEM spectra has appeared. In particular, as the BEEM current at a given voltage depends both on the Schottky barrier height and the ballistic electron transport in the base, the separation of these two effects is of importance. In this paper, we work out fully analytical expressions of the BEEM spectra based on the Bell-Kaiser model [4], that allow fitting the experimental data in the full range of voltages. We demonstrate this on spectra

[a] e-mail: thiaville@lps.u-psud.fr

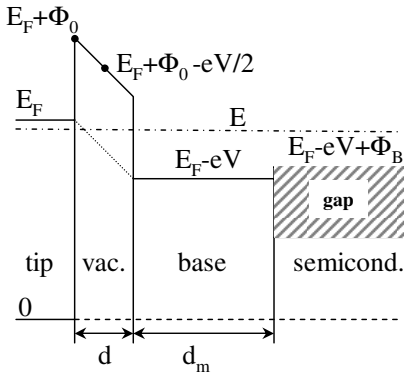

Fig. 1. Definition of electron energies for the biased metal/vacuum/metal/semiconductor junction. The absolute value of the electron charge is denoted by e.

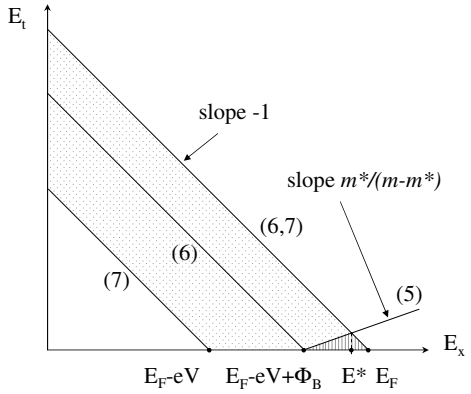

Fig. 2. Representation, in the (E_x, E_t) space (so-called phase space) of the electronic states that contribute to the tunnel current (dotted and hatched regions) and to the BEEM current (hatched region only). Numbers refer to the corresponding equations in the text.

acquired at room temperature from Au/Si(111) samples prepared by different procedures. The observed BEEM contrasts are shown to result from both Schottky barrier shifts and variations of the ballistic electrons transmission. This fitting is also compared to results of much more complex calculations from the literature.

2 BEEM current calculation

In order to explain how analytical expressions for the relative BEEM current are obtained, we need first to recall the Bell-Kaiser model, also called phase-space model [4]. The simplifying assumptions that allow analytical calculations are also discussed.

2.1 Phase space model [4]

The calculations framework is planar tunneling, as in all theoretical BEEM models [3] up to now. Physically, tunneling from the STM tip is anticipated to only modify the weight of the electron waves injected with a non-zero transverse momentum. Electron states are described in the absence of atomic scale lattice potentials, i.e. in the free electrons approximation. An effective mass m^* is introduced for the semiconductor, independent of the wavevector (isotropic and energy independent mass). For the metal, one assumes that m is the electron mass. This assumption is not critical, as the formulae will be seen to depend only on the masses' ratio. Electron energies are counted with respect to the bottom of the conduction band in the tip (Fig. 1). A potential V is applied to the sample (the tunnel voltage). An electron state with energy E has, in the tip, a wavevector $\mathbf{k} = (k_x, \mathbf{k}_\mathrm{t})$, where x is the coordinate normal to the layers and t stands for the plane of the layers. The free electrons model implies that

$$0 \leqslant E = \frac{\hbar^2}{2m}\left(k_x^2 + \mathbf{k}_\mathrm{t}^2\right) \equiv E_x + E_\mathrm{t}, \qquad (2)$$

where the axial and transverse parts of the (kinetic) energy are denoted by E_x and E_t, respectively. At the semiconductor surface, this energy state will satisfy (see Fig. 1)

$$E = \frac{\hbar^2}{2m^*}\left((k_x')^2 + \mathbf{k}_\mathrm{t}^2\right) + E_\mathrm{F} - eV + \Phi_\mathrm{B}. \qquad (3)$$

Implicit in (3) is the very important assumption of a perfect interface transmission, that implies the conservation of the transverse wavevector $\mathbf{k}_\mathrm{t}$. In the metallic base one writes similarly to (2)

$$E = \frac{\hbar^2}{2m}\left((k_x'')^2 + \mathbf{k}_\mathrm{t}^2\right) - eV. \qquad (4)$$

Again, the assumption of $\mathbf{k}_\mathrm{t}$ conservation at the vacuum-metal interface holds for a perfectly flat situation. Eliminating E between (2) and (3) results into

$$\begin{aligned} E_\mathrm{t} &= \frac{m^*}{m-m^*}\left(E_x - E_\mathrm{F} + eV - \Phi_\mathrm{B} - E_x'\right) \\ &\leqslant \frac{m^*}{m-m^*}\left(E_x - E_\mathrm{F} + eV - \Phi_\mathrm{B}\right). \end{aligned} \qquad (5)$$

The lower effective mass in the semiconductor gives rise to a limitation of transverse momentum, similar to the total reflection effect for optical waves. The second constraint for the energies E_x and E_t comes from the occupation of energy states. At zero temperature, it reads

$$E_\mathrm{min} \equiv E_\mathrm{F} - eV + \Phi_\mathrm{B} \leqslant E_x + E_\mathrm{t} \leqslant E_\mathrm{F}. \qquad (6)$$

These limits are drawn in Figure 2, in the (E_x, E_t) space. For the tunneling into the base, the limits are less severe

$$E_\mathrm{T} \equiv E_\mathrm{F} - eV \leqslant E_x + E_\mathrm{t} \leqslant E_\mathrm{F}. \qquad (7)$$

Figure 2 shows that ballistic electrons entering into the semiconductor have a maximum transverse energy, obtained for

$$\begin{aligned} E_x = E^* &\equiv \frac{m^*}{m}E_\mathrm{min} + \left(1 - \frac{m^*}{m}\right)E_\mathrm{F} \\ &= E_\mathrm{F} - \frac{m^*}{m}\left(eV - \Phi_\mathrm{B}\right). \end{aligned} \qquad (8)$$

This transverse energy, and thus momentum, limitation is the reason of the spatial resolution of BEEM as a microscopy ('searchlight' effect [9]).

2.2 Currents calculation

The tunneling (I_T) and BEEM (I_B) currents are calculated using the semi-classical model first introduced by Sommerfeld and Bethe [10,11]. A tip electron state $(k_x, \mathbf{k}_\mathrm{t})$ carries a x current proportional to k_x. As the density of states in the $\mathbf{k}$ space is uniform, integration of the electric current over the states involves $k_x dk_x dk_y dk_z \propto dE_x dE_\mathrm{t}$, using the revolution symmetry in the transverse plane. The geometry of integration is depicted in Figure 2. The function to be integrated over the allowed surface is the transmission probability of the electrons.

This transmission is written as a product of factors, namely the partial transmission at the various interfaces and through the layers.

– The *transmission under the tunnel barrier* is, in the WKB approximation [12],

$$T_\mathrm{tunnel} \propto \exp\left[-2d\frac{\sqrt{2m\left(\Phi_0 - eV/2 + E_\mathrm{F} - E_x\right)}}{\hbar}\right], \tag{9}$$

where Φ_0 is the work function of the metal. For axial electron energies close to E_F, the tunnel transmission is approximated by

$$T_\mathrm{tunnel} \approx T_0(V)\exp\left[-\frac{E_\mathrm{F} - E_x}{E_0}\right] \tag{10}$$

with a characteristic energy E_0 reading

$$E_0(V) = \frac{\hbar}{d}\sqrt{\frac{\Phi_0 - eV/2}{2m}}. \tag{11}$$

This is one of the main assumptions underlying the full analytical calculation of the BEEM spectra. Using typical values $d = 1$ nm and $\Phi_0 = 4$ eV, one finds a weak dependence of E_0 on tunnel voltage: E_0 is 0.39, 0.37 and 0.34 eV, for tunnel voltages 0, 1 and 2 V, respectively. The tunnel transmission concentrates its weight at the apex $E_x = E_\mathrm{F}$ of the triangle shown in Figure 2. Note that a wave transmission coefficient should be included as a prefactor in (9), proportional to $\left(\Phi_0 - eV/2 + E_\mathrm{F} - E_x\right)/E_x$ (the x wave vector inside the barrier being small compared to k_x). This factor would be changed also when going beyond the planar tip approximation. However, the E_x dependence of this prefactor is weak compared to that in the exponential part of T_tunnel.

– A similar factor for current *transmission at the base/substrate interface* exists [5], given by

$$T_\mathrm{int} = \frac{4k_x'' k_x'}{\left(k_x'' + k_x'\right)^2} = 1 - \left(\frac{k_x' - k_x''}{k_x' + k_x''}\right)^2. \tag{12}$$

As $\hbar^2(k_x')^2/2 = m^*\left(E_x - E_\mathrm{min}\right) - \left(m - m^*\right)E_\mathrm{t}$ and $\hbar^2(k_x'')^2/2 = m\left(E_x + eV\right)$, one sees that this factor goes to zero at the limit (5), providing a smooth cutoff in the (E_x, E_t) integration.

– Finally, a *hot electron transmission across the metal base* T_met has to be introduced. It is generally written in the form of an exponential decay with an attenuation length λ [9] whose spin dependence gives the BEMM contrast [13]

$$T_\mathrm{met} = \exp\left(-d_\mathrm{m}/\lambda\right). \tag{13}$$

The attenuation length is anticipated to depend on the electron energy above the Fermi level in the metal. One should be aware that this expression is already a huge simplification, considering the variety of processes affecting hot electrons transport (elastic and inelastic scattering, for example). As far as the integration over the phase space is concerned, this transmission amounts to a constant multiplicative factor. Indeed, hot electrons contributing to the BEEM current have an energy excess between eV and $eV - E_0$, typically (see Fig. 1). For the BEEM spectrum however, a $\lambda(eV)$ dependence results in a shape distortion.

In the following, we fit experimental spectra under the assumption that an overall *constant* transmission factor T exists

$$T = T_\mathrm{int}T_\mathrm{met} \tag{14}$$

(the prefactor $T_0(V)$ in the tunnel transmission disappears in the currents ratio). An effective value for T will be returned from the fits. This precludes the discussion of the energy dependent processes described above, considered to be a next-order effect at this stage. Note that the transmission T defined here is equivalent to the parameter R introduced by Bell and Kaiser [4], whose value was however not exploited.

From the re-derivation of the phase space model presented above, we expect that $T < 1$ will be always found. This basically holds as long as the transverse momentum is conserved. If not the case, only energy conservation would restrict the BEEM current. Using the phase space diagram of Figure 2, this would mean that the allowed surface for the BEEM current is increased to the full right-hand band $E_\mathrm{F} - eV + \Phi_\mathrm{B} < E_x + E_\mathrm{t} < E_\mathrm{F}$, so that the relative BEEM current increases. An alternative view of partial conservation of the transverse momentum consists in having m^* closer to m, as this also increases the surface of the BEEM current phase space triangle. The effect of a larger m^* is addressed below.

2.3 Sharp cutoff

The integration with sharp cuts (i.e. zero temperature and $T_\mathrm{int} = T_\mathrm{met} = 1$) is immediate, resulting in

$$I_\mathrm{T} = C\left[1 - \exp\left(-\frac{eV}{E_0}\right) - \frac{eV}{E_0}\exp\left(-\frac{E_\mathrm{F}}{E_0}\right)\right] \tag{15}$$

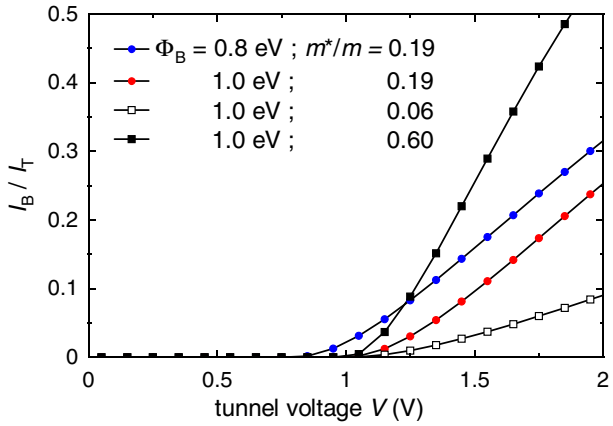

Fig. 3. (Color online) Calculated relative BEEM current spectra in the free electrons model (parameters for for the metal $E_F = 4$ eV, tunnel transmission decay energy (Eq. (11)) $E_0 = 0.4$ eV). The Schottky barrier height Φ_B and the semiconductor effective mass m^* are varied. The temperature is zero (sharp cutoff model), and the transmissions T_{int} and T_{met} are set to unity.

for $0 \leqslant eV \leqslant E_F$, and

$$I_B = C\left[1 - \frac{m}{m-m^*}\exp\left(-\frac{m^*}{m}\frac{eV-\Phi_B}{E_0}\right) + \frac{m^*}{m-m^*}\exp\left(-\frac{eV-\Phi_B}{E_0}\right)\right] \quad (16)$$

for $\Phi_B \leqslant eV \leqslant E_F$. Figure 3 plots the relative BEEM current I_B/I_T versus tunnel voltage V for typical values of the other parameters. Above the threshold, the current rises quasi-linearly, as seen in the experiments [4] for this voltage range. Saturation occurs at higher voltages, of the order of E_F/e. The effect of the main parameters Φ_B and m^*/m can be clearly seen in Figure 3: varying the Schottky barrier mainly shifts the spectrum without deformation, whereas the linear rise above the threshold is controlled by the effective mass m^*.

2.4 Effect of temperature

The consideration of a non zero temperature is not difficult within the present framework. In order to perform the calculations analytically, we take an exponential approximation for the Fermi distribution function ($f_F(\xi) = 1/(1+e^{\xi})$), namely

$$f(\xi) \approx 0.5e^{-a\xi} \text{ if } \xi > 0$$
$$\approx 1 - 0.5e^{a\xi} \text{ if } \xi < 0, \quad (17)$$

where $\xi = (E - E_F)/k_B\Theta$ and Θ is the absolute temperature. This approximation is very good for $a = 0.7$.

Referring to the energy diagram of Figure 1, the finite temperature will only affect the energy distribution of the electrons emitted by the tip. Indeed, the constraints for electron injection into the semiconductor are not due to occupied states, but to the structure of the conduction band. Thus, in the phase space picture of Figure 2, only the limit (5) becomes blurred. Expression (17) shows that, compared to the sharp cutoff, we only need to add the contribution of the exponentials on both sides of this straight line (depicted as (5) in Fig. 2). The calculations are lengthy but straightforward. Introducing the non-dimensional variable

$$\alpha = \frac{aE_0}{k_B\Theta} \quad (18)$$

and the sign $\sigma = \text{sgn}(eV - \Phi_B)$, the additional tunnel and BEEM currents read

$$\Delta I_T = C\left[\frac{1-e^{-eV/E_0}}{\alpha^2-1} + \frac{e^{\alpha eV/E_0}-1}{2\alpha(\alpha+1)}\exp\left[-(\alpha+1)E_F/E_0\right]\right] \quad (19)$$

and

$$\Delta I_B = \frac{C}{2}\left[-\frac{\sigma\frac{m^*}{m}\exp\left[-(\alpha\sigma+1)\frac{eV-\Phi_B}{E_0}\right]}{(\alpha+\sigma)(\alpha+\sigma(1-m^*/m))} + \left(\frac{1}{\alpha-1}-\frac{1}{\alpha+\sigma}\right) + \exp\left(-\frac{m^*}{m}\frac{eV-\Phi_B}{E_0}\right) \times \left(\frac{1}{\alpha+1-m^*/m}-\frac{1}{\alpha-\sigma(1-m^*/m)}\right)\right], \quad (20)$$

where C is the same as in (15,16).

Figure 4 displays the calculated BEEM spectra when taking into account a finite temperature (here $\Theta = 300$ K). It can be seen that temperature affects only a narrow voltage region, of width ≈200 mV at 300 K (i.e. $\pm 4k_B\Theta$). The relative BEEM current takes off at a lower voltage. The quasi-linear slope above the threshold is however not affected. From these results, one concludes that the consideration of the 'thermal broadening' effects is important only in close vicinity of the BEEM threshold. Temperature effects matter for example when trying to measure the exponent of the power law quoted before, as a thermal broadening obviously decreases the threshold and increases the exponent. If the full spectrum is analysed, however, the temperature effect is anticipated to be weak. In fact, fitting by the sharp cutoff expressions the values obtained with a non-zero temperature gives only tiny differences in threshold voltage and slope (see Fig. 4).

2.5 Comparison to more elaborate models

The formulae derived above cannot pretend taking into account all the details of the physics relevant to BEEM. Without being exhaustive, some obvious shortcomings of the model are: the absence of the relevant conduction band valleys, a constant effective mass (no anharmonicity, anisotropy between longitudinal and transverse

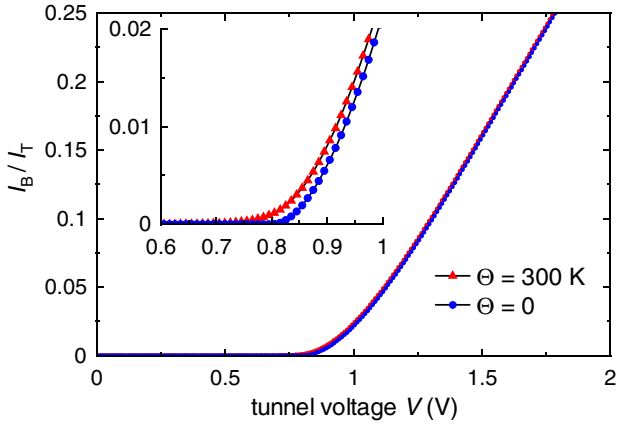

Fig. 4. (Color online) Calculated relative BEEM current spectra in the free electrons model (same parameters as in Figure 3 with $\Phi_B = 0.8$ eV and $m^*/m = 0.19$), with the inclusion of a non zero temperature. The fit, by the model at zero temperature, of the 300 K values results into $\Phi_B = 0.791$ eV and a relative transmission $T = 0.995$. The inset shows a zoom on the threshold region.

components of the wavevector), an energy-independent E_0 parameter, an energy and wavevector independent transmission coefficient, etc.

However, comparing to a rather complex model with microscopic ingredients [3], itself compared to experimental results for 7.5 nm Au/Si(111) at 77 K [14], we find a nice agreement using our standard parameters, i.e. $E_F = 4$ eV, $E_0 = 0.4$ eV and $m^*/m = 0.19$, supplemented by $\Phi_B = 0.85$ eV and $T = 0.2$.

Comparing to another model [15] that includes non-anharmonicity and interface scattering, again matched to the same experimental results, we find that we can get the same results using the parameters of that model, namely $\Phi_B = 0.8$ eV and $m^*/m = 0.33$, together with $E_0 = 0.4$ eV and $T = 0.6$.

Thus, we conclude that the formulae we obtained, with just a few parameters, can be applied to reproduce a quite complex reality. The obtained values of the transmission are also reasonable.

3 Application to experiments

These simple formulae have been applied to the analysis of BEEM spectra obtained [16] on Au/Si(111) samples. The BEEM microscope is a modified Omicron STM-1 (a back contact to the sample plate was added, connected to a second in-vacuum $I-V$ converter). It allows for BEEM spectroscopy and imaging in UHV conditions (low 10^{-10} mbar range) at room temperature. Spectra were acquired in the closed loop feedback mode: for each voltage applied the tip is first moved vertically so as to keep the tunnel current to the setpoint value. Note that the tip displacement incurred is rather small, a factor of 10 in tunnel resistance corresponding to a tip retraction of 1 Å [17]. The success of the regulation can be monitored by looking at the recorded $I_T(V)$ spectrum. After every V increase, a waiting time of 50 ms preceded the 40 ms data acquisition time, so as to let the tip stabilize.

The model parameters assumed for the fits are $E_0 = 0.4$ eV (the value discussed above), $E_F = 4$ eV and $m^*/m = 0.19$. This last number is the tabulated [18] value for the transverse effective mass of silicon, for a conduction band with bottom state having a wavevector along the [100] direction. As our sample surface has a (111) orientation, this band is not appropriate. However, as shown early [19], experimental spectra for Au on Si(100) and Si(111) surfaces are unexpectedly similar. The thorough understanding of this effect is still a matter of controversy, two mechanisms having been proposed, namely interface scattering [15,19] and electron transport through a (111) textured gold film [20].

Two parameters are obtained from the fits, namely the Schottky barrier height Φ_B and the multiplicative factor T introduced earlier (14), that we call transmission and obtain as

$$\frac{I_B}{I_T}\Big|_{exp} = T \times \frac{I_B}{I_T}\Big|_{model}, \qquad (21)$$

where the model terms are (16)/(15) for the 'sharp cutoff' case, and (16) + (20)/(15) + (19) for the non-zero temperature case. The factor T, assumed not to depend on the tunnel voltage V, represents the global effect of (i) the quantum-mechanical wave transmission coefficient at the various interfaces, mainly the metal/semiconductor interface and (ii) the ballistic electrons transmission across the gold film (see Sect. 2.2).

3.1 Au/Si(111) samples prepared by UHV evaporation

Si(111)-H surface

The Si(111)-H surface was prepared chemically, following the established procedure [21]. After immediate introduction into the chamber, a gold layer was evaporated at room temperature from a Mo crucible heated by an electron beam (the vacuum in that chamber attached to that of the STM was at most 3×10^{-10} mbar during evaporation). The Schottky contact area was restricted by a shadow mask placed ≈3 mm in front of the sample surface, to a 3×0.4 mm^2 rectangle. The evaporation rate was measured by a calibrated quartz microbalance to be ≈4 nm/h. Following UHV gold evaporation, the sample was transferred to a separate chamber (DC diode sputtering) in which a thick (150 nm) gold dot was positioned on the upper end of the Schottky contact. After microbonding this dot to the sample plate, the sample was introduced again in the UHV chamber for BEEM measurements.

Figure 5 shows a typical spectrum for a 7.5 nm thick gold layer. The tunnel current I_T (right scale) is well regulated at 1 nA ±1%. The ratio of the simultaneously measured I_B to I_T is plotted on the left scale. The curve superposed to the data points is a least squares fit to the 'sharp' model described above (15, 16). This model is seen to reproduce the data extremely well. It provides

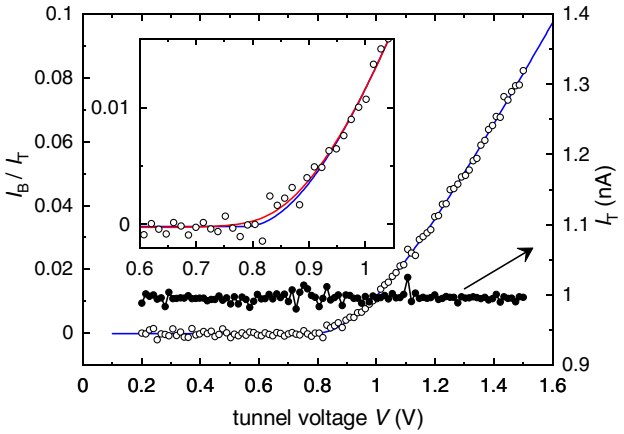

Fig. 5. Experimental BEEM spectrum acquired at one position of the Au/Si(111)-H interface (nominal tunnel current: 1 nA). The measured tunnel current is shown on the right scale, and the relative BEEM current on the left. Only the fit of this ratio with the "sharp" model is displayed on the main figure, and both fits (see text) can be distinguished in the zoom shown in the inset.

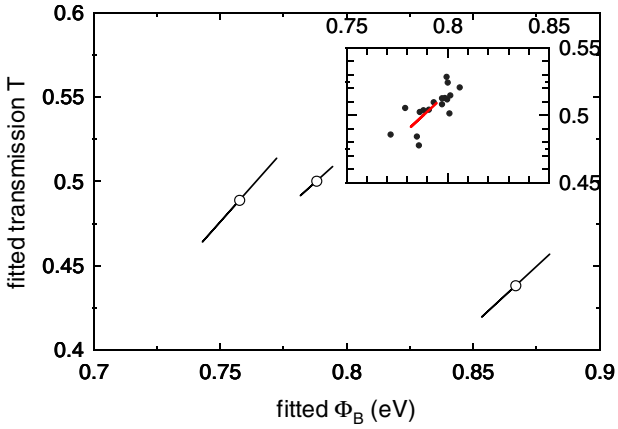

Fig. 6. Distribution of the fitted Schottky barrier and sample transmission for a 7.5 nm Au/Si(111)-H sample. For each of the 3 spectra, the accuracy of the parameters determination is shown by a single inclined error bar, as explained in the text. The inset shows the effect of an added noise of amplitude 0.02 to the experimental curve of Figure 5 (corresponding to the central point of the graph), so as to generate a distribution of (Φ_B, T) couples. The fit results of the original data with correlated error bars are also included in the inset, demonstrating the adequacy of the latter.

$\Phi_B = 0.788$ eV, with a 95% confidence interval [0.775–0.801], and $T = 0.5$ with an interval [0.492–0.509]. Inclusion of the finite temperature (room temperature here) changes the values only slightly: $\Phi_B = 0.800$ eV (interval [0.794–0.807]), and $T = 0.507$ (interval [0.498–0.516]). Indeed, as the fit is performed over an extended voltage range, the influence of the temperature, as it exists only close to the threshold, is minimized. This insensitivity is one advantage of using our model, instead of a simple power law, for the determination of the Schottky barrier. A zoom around the threshold region, displayed in the inset, shows the quite small difference between both fits. Given the noise present in this single spectrum, recorded with a low tunnel current, we can consider that the refinement brought by the thermal broadening is not important, even in that region.

Other BEEM spectra were acquired on the same image. In order to study how Φ_B and T vary from place to place, we plot in Figure 6 the fitted values for these quantities. The error bars are displayed not as independent (a cross at every point), but as strongly coupled, with 2 inclined neighbours for every point. Indeed, it is obvious that if a higher Φ_B is forced into a fit, a higher T will be found (see also Fig. 10 later). In a statistical language, the fitting routine returns a positive correlation coefficient, close to 1, between these two parameters. Practically, fitting the same spectrum with various noise realizations with similar amplitude gives rise to (Φ_B, T) couples that scatter along that inclined segment, as demonstrated in the inset of Figure 6. Although the correlation between T and Φ_B is not strong, a lower transmission is seen for the higher Schottky barrier. As such a behaviour was also seen on samples with a tunnel barrier inserted inside the base [22], this may be the interpretation of our measurements.

Technological Si(111) surface

Data for another sample prepared also in UHV conditions are now discussed. Compared to the previous sample, the Si surface is not quoted to be hydrogenated, as the hydrogenation procedure was applied to the surface within a window opened in a thick SiO_2 (≈500 nm) film by optical lithography and wet etching. As a consequence, surface hydrophoby after hydrogenation could not be seen (the silicium oxide is hydrophilic) and STM observation before Au evaporation did not reveal atomic terraces as for the previous sample. Figure 7 shows 16 spectra acquired during the same image. The raw data are shown in (a), and the spectra corrected for variations of Φ_B and T in (b). Compared to the previous sample, the noise is more important. This is attributed to a lower Schottky junction resistance, resulting in a larger Johnson noise.

The distribution of the resultant effective Schottky barrier Φ_B and transmission T is displayed in Figure 8. This sample shows, on top of a large scatter of these parameters, a tendency for an increase of T with larger Φ_B, which is opposite to that of the previous sample. This tendency is confirmed by the inclusion in the distribution of the fitted parameters obtained for spectra taken at large and low BEEM current spots in the image (Fig. 9). Incidentally, this graph displays effective transmissions that are found larger than unity whereas, from the model derivation, we would expect $T < 1$. However, any atomic-scale roughness of the metal-semiconductor interface breaks the translation invariance on which the conservation of the transverse momentum rests. As this conservation restricts in phase space the electrons that can be collected in the semiconductor (see Fig. 2), it is clear

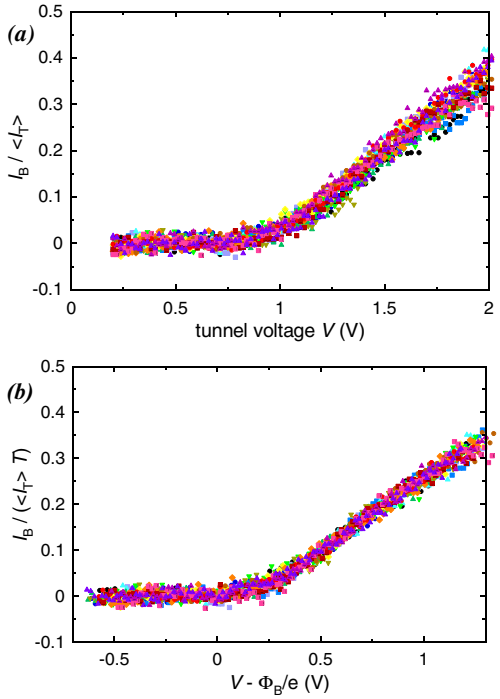

Fig. 7. (Color online) Experimental BEEM spectra acquired at 16 positions of a 16 nm Au/Si(111) junction, within a window opened in a thick SiO_2 film (nominal tunnel current: 2 nA). (a) Raw data and (b) data corrected for variations of effective Schottky barrier and transmission, effectively reducing the data scatter.

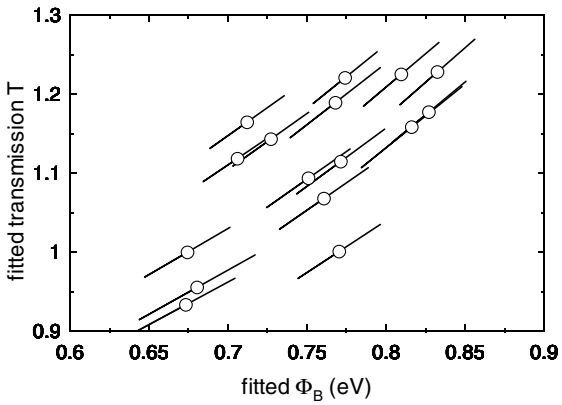

Fig. 8. Distribution of the fitted Schottky barrier and sample transmission for the 16 nm Au/Si(111) 'technological' sample. For each spectrum, the accuracy of the parameters determination is again shown by an inclined error bar. The point-to-point variation of the fitted parameters is about three times as large as their undetermination.

that interface roughness can give rise to a larger effective transmission, as already discussed [15].

3.2 Au/Si(111) samples prepared by sputtering

Samples were also prepared by sputtering gold on a hydrogenated Si(111) surface. The sputtering was performed

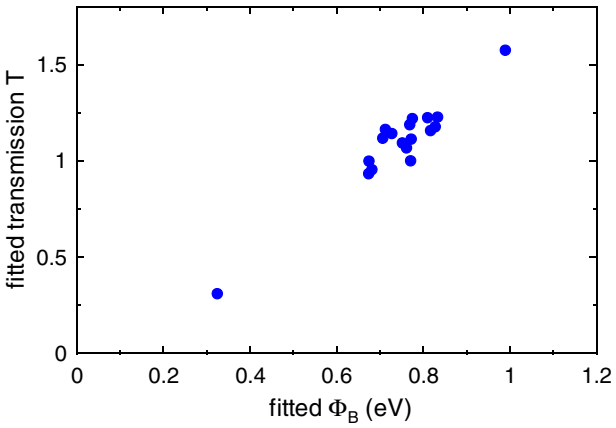

Fig. 9. Correlation of Schottky barrier and sample transmission for the 16 nm Au/Si(111) 'technological' sample. Spectra acquired at locations with high and low BEEM current are included.

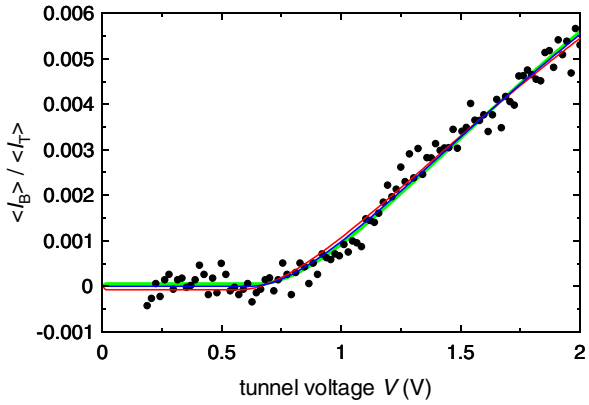

Fig. 10. (Color online) Experimental BEEM spectrum (average of 3 positions) of a 5 nm Au/Si(111)-H junction prepared by sputtering (nominal tunnel current: 18 nA). The adjustment (blue line) gives a low effective Schottky barrier (0.62 eV, interval [0.58, 0.66]) and a low effective transmission (0.015, interval [0.014, 0.016]). The adjustments with a Schottky barrier fixed at the lower (red line) and higher (green line) values are included for comparison.

in the DC diode configuration, with no magnetron and under a high Ar_2 pressure (0.1 mbar), the chamber base pressure being a few 10^{-6} mbar. As already clear from macroscopic $I(V)$ measurements, such Schottky junctions have a low effective barrier. This is confirmed by the local BEEM spectra, as shown in Figure 10. The low Schottky barrier may be attributed to interface alloying. Moreover, BEEM spectroscopy reveals a low effective transmission. It is attributed to a very disordered gold film (with Ar gas inclusions and/or cavities).

4 Conclusion

In this work, we have applied the simple phase space model of Bell and Kaiser to Schottky diodes prepared on Si(111)

from ultrathin Au layers deposited and patterned by different techniques. From a full analytical calculation of the tunnel and BEEM currents that was developed under some simplifying assumptions, we could fit the experimental spectra extremely well and deduce precise values for the effective Schottky barrier as well as an effective transmission that we defined. These fitting formulae have the advantage, over previous too simple expressions, of applying to a wide range of voltages and allowing taking the best out of the simple physical assumptions made in the phase space model. A systematic difference in barrier height and transmission was observed depending on fabrication procedure. In view of the recent developments of magnetic BEEM (BEMM), we believe that this model may be of some help.

The authors would like to thank M. Bernheim from this laboratory for his help in the preparation of the Si-H surfaces. This research was supported by NEDO (International research grant *Nanopatterned magnetic systems: magnetic structures and dynamical behaviors*) and the French Action NANODYNAMAG.

References

1. W. Kaiser, L. Bell, Phys. Rev. Lett. **60**, 1406 (1988)
2. V. Narayanamurti, M. Kozhenikov, Phys. Rep. **349**, 447 (2001)
3. P. de Andres, F. Garcia-Vidal, K. Reuter, F. Flores, Prog. Surf. Sci. **66**, 3 (2001)
4. L. Bell, W. Kaiser, Phys. Rev. Lett. **61**, 2368 (1988)
5. M. Prietsch, R. Ludeke, Phys. Rev. Lett. **66**, 2511 (1991)
6. M. Cuberes, A. Bauer, H. Wen, D. Vandré, M. Prietsch, G. Kaindl, J. Vac. Sci. Technol. B **12**, 2422 (1994)
7. H. Palm, M. Arbes, M. Schulz, Phys. Rev. Lett. **71**, 2224 (1993)
8. W. Rippard, R. Buhrman, Appl. Phys. Lett. **75**, 1001 (1999)
9. M. Prietsch, Phys. Rep. **253**, 163 (1995)
10. A. Sommerfeld, H. Bethe, in *Handbuch der Physik*, edited by H. Geiger, K. Scheel (Julius Springer, Berlin, 1933), Vol. 24/2
11. J. Simmons, J. Appl. Phys. **34**, 1793 (1963)
12. S. Gasiorowicz, *Quantum Physics* (Wiley, New York, 2003)
13. W. Rippard, R. Buhrman, Phys. Rev. Lett. **84**, 971 (2000)
14. L. Bell, Phys. Rev. Lett. **77**, 3893 (1996)
15. D. Smith, E. Lee, V. Narayanamurti, Phys. Rev. Lett. **80**, 2433 (1998)
16. F. Caud (2006), Ph.D. thesis, Université Paris-sud, `http://tel.ccsd.cnrs.fr`
17. *Scanning Tunneling Microscopy I*, edited by R. Wiesendanger, H. Güntherodt (Springer, Berlin, 1993)
18. S. Sze, *Physics of semiconductor devices* (Wiley, New York, 1981)
19. L. Schowalter, E. Lee, Phys. Rev. B **43**, 9308 (1991)
20. F. Garcia-Vidal, P. de Andres, F. Flores, Phys. Rev. Lett. **76**, 807 (1996)
21. G. Higashi, R. Becker, Y. Chabal, A. Becker, Appl. Phys. Lett. **58**, 1656 (1991)
22. W. Rippard, A. Perella, R. Buhrman, Appl. Phys. Lett. **78**, 1602 (2001)